Swiss Journal of Geosciences (2019) 112:579–596
https://doi.org/10.1007/s00015-019-00350-5

Geochemical constrains on dolomitization pathways of the Upper Jurassic carbonate rocks in the Geneva Basin (Switzerland and France)

Y. Makhloufi[1] · E. Samankassou[1]

Received: 1 February 2019 / Accepted: 6 October 2019 / Published online: 5 November 2019

Abstract
The Kimmeridgian-Tithonian carbonate rocks of the Geneva Basin represent potential reservoirs for geothermal energy exploitation. Based on petrographic data, a previous study (Makhloufi et al. 2018) reported three different stages of dolomitization affecting these carbonate rocks, followed by dedolomitization. The present study focuses on the geochemical characterization of these stages based on O, C and Sr isotopes of dolomites and dedolomites. The oxygen isotopic values of early dolomite are depleted compared to the values of Late Jurassic marine cements. This is interpreted to reflect dolomite precipitation from an oxygen-enriched fluid, likely evaporitic. Carbon isotopic values are close to the composition of well-preserved Late Jurassic cements suggestive of abiotic precipitation. These findings are consistent with a scenario of reflux type dolomitization induced by high-frequency sea-level changes producing pulses of dolomitizing brines. Late dolomitization represents an advanced level of replacement. Isotopic data exhibits depleted oxygen composition pointing towards burial diagenesis and is interpreted as the results of shallow burial over-dolomitization. Ages provided by radiogenic strontium isotopes data are consistent with an early first stage of dolomitization followed by late burial dolomite. Dedolomitization is observed at different orders of magnitude and might results from the interaction with meteoric water initiating the dissolution of both early and late dolomites. This dedolomitization would have taken place during long-term emersion events or after the exhumation. The results presented in this work provide further understanding of the processes involved in dolomitization under the influence of high-frequency sea-level fluctuations and the evolution of dolomitic fabrics during burial.

Keywords Early diagenesis · Dolomite · Dedolomite · Seepage-reflux · Upper Jurassic · Geneva Basin

1 Introduction

The Upper Jurassic limestones of the Geneva Basin represent one the major active aquifers and is currently evaluated for geothermal energy exploitation. It has been shown that the Upper Jurassic, and specifically the Kimmeridgian units, are affected by dolomitization and dedolomitization processes (Fondeur et al. 1954; Shearman et al. 1961; Makhloufi et al. 2018). Such diagenetic processes are commonly associated with important modifications in the reservoir properties of the rock by poro-genesis or poro-necrosis mechanisms (Schmoker et al. 1985; Braithwaite 1991; Giorgioni et al. 2016).

Several studies discussed the scenarios and pathways of dolomitization of the Upper Jurassic limestones for the Molasse Basin, from the western part of Switzerland and France in the Geneva Basin (Rameil 2008), to the eastern part of the basin in southern Germany (Reinhold 1998). In the Geneva Basin, only the Jura Mountains were considered, and the southern part of the basin was not taken into account. Moreover, previous work showed that the Upper Jurassic of the Geneva Basin exhibits an important volume of sucrosic dolomite (Makhloufi et al. 2018) which origin and precise timing of formation has not been determined yet. In the same way, the timing and origin of dedolomites

Editorial Handling: W. Winkler.

Electronic supplementary material The online version of this article (https://doi.org/10.1007/s00015-019-00350-5) contains supplementary material, which is available to authorized users.

✉ Y. Makhloufi
yasin.makhloufi@unige.ch

[1] Department of Earth Sciences, University of Geneva, Rue des Maraîchers 13, 1205 Geneva, Switzerland

observed in the Upper Jurassic units are poorly constrained. Due to their characteristics, both the sucrosic dolomites and the dedolomites represented level of economic interest especially in the context of geothermal energy exploitation.

The present study is a follow up of Makhloufi et al. (2018). Petrographic analyses allowed to constrain the paragenesis of the Upper Jurassic units and revealed that all units experienced several stages of dolomitization. The initial petrographic results pointed to two dolomitization events: an early reflux-type dolomitization and a later burial dolomitization. Dedolomitization, through calcitization and/or dissolution was also identified and reported to be creating important volume of secondary pore space. Dedolomitization can be associated to two processes (Ayora et al. 1998): (1) a one-step or replacement process, involving the dissolution of dolomite coupled with formation of calcite (Evamy 1967) and/or (2) a two-step process involving dissolution of dolomite resulting in secondary pore space, and later precipitation of calcite either during the same overall process (Warrak 1974; Kenny 1992), or from a different solution at a different time (Jones et al. 1989; James et al. 1993).

This initial study served as a reasonable framework for geochemical analyses in order to constrain the nature and timing of fluid migration as well as the scenarios and hypotheses for the most likely pathways of dolomitization discussed therein.

The data presented here are the results of detailed outcrop studies, sampling and the use of isotope geochemical analyses. The objectives are: (1) to test and provide more insights on the models of dolomitization and dedolomitization proposed in Makhloufi et al. (2018), (2) to compare the likely scenarios with previously proposed models in similar settings, (3) to constrain the origin for the pore fluids responsible for the different stages of dolomitization and dedolomitization and (4) to propose a timing for the formation of dolomite and dedolomites. Furthermore, the results presented here are compared with literature data at the regional and global scales in addition to proposing a database of 250 isotopic values of calcite, dolomite and dedolomite cements that can be used by the wider scientific community.

2 Geologic and sedimentologic setting

The Geneva Basin is located at the Swiss-French transnational zone in the south-west of Lake Geneva. The basin is bordered to the north-east by the internal chain of the Jura Mountain and to the south-east by the front of the Alpine units (Fig. 1). The basin lies on a Variscan crystalline basement with a sedimentary cover of Mesozoic to Cenozoic succession about 3000 to 5000 meters thick. The Mesozoic series are mainly composed of carbonates and marls, along with evaporites (Enay 1969; Bernier and Enay 1972; Bernier 1984). During the Triassic, when the basin was connected to the Tethys Ocean, a marine transgression led to the deposition of thick evaporitic series (Disler 1914). The Lower Jurassic deposits also record a transgressive trend with open-marine conditions prevailing until the Aalenian (Sommaruga 1997). The Middle Jurassic succession is characterized by a first regressive trend and a shift towards shallower conditions during the Bajocian and Bathonian (Strasser 1994). The Upper Jurassic deposits are results of a second regressive trend while a shallow carbonate platform developed and extended towards the northwest. During the Kimmeridgian, major change in depositional environment induced the growth of patch reefs on top of pre-existing structural highs (Meyer 2000). The inter-reef depressions were then sealed during the Tithonian by prograding tidal deposits followed locally along with immersive facies (Strasser 1988).

The Kimmeridgian and Tithonian (Upper Jurassic) of the Geneva Basin are subdivided in six formations outcropping in the Jura Mountains, Mount Salève and Mount Vuache (Charollais et al. 2013). These are the *Couches à Céphalopodes, Calcaires de Tabalcon, Complexe Récifal, and Tidalites de Voulgans*. The *Complexe Récifal* consists of three subunits: the *Calcaires Récifaux*, *Calcaires Plaquetés*, and *Calcaires de Landaize* subunits. Readers are referred to Makhloufi et al. (2018) for an extended description of the studied sections. The stratigraphic sections and position of the samples analyzed are displayed in Fig. 1.

During the late Cretaceous, several depositional environments and overall shallow and warm-water conditions prevailed (Charollais et al. 2013; Sommaruga 1997) leading to the deposition of bioclastic limestones, bioturbated limestones and marls rich in organic matter. Lower Cretaceous deposits are not recorded in the Geneva Basin, probably due to their emersion and later erosion during the Paleocene. This erosion led to the development of an important karstic system, which will be filled during the Eocene by the "sidérolithique" red sandstone formation (Sommaruga 1997). The Alpine phase and the associated foreland tectonic regime will induce de deposition of a thick Oligocene–Miocene detrital-rich unit called the "Molasse" (Favre et al. 1880; Heim 1922; Charollais et al. 2007).

3 Materials and methods

Powder samples for geochemistry were obtained using a 0.3 mm drill bit mounted on a Dremel© rotary workstation. Samples consists of bulk ($n = 24$) and selected

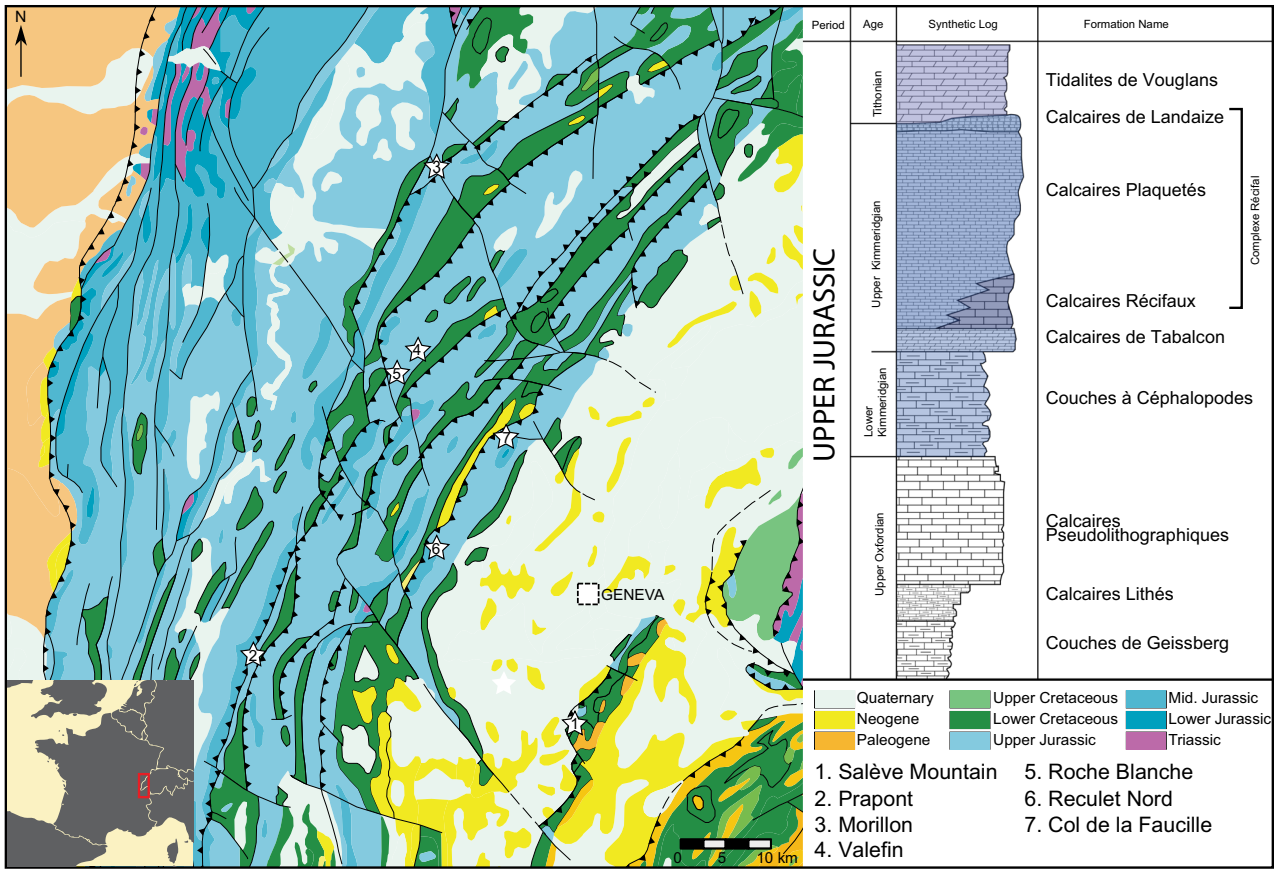
N
GENEVA
0 5 10 km
Period
Age
Synthetic Log
Formation Name
UPPER JURASSIC
Tithonian
Upper Kimmeridgian
Lower Kimmeridgian
Upper Oxfordian
Tidalites de Vouglans
Calcaires de Landaize
Calcaires Plaquetés
Calcaires Récifaux
Complexe Récifal
Calcaires de Tabalcon
Couches à Céphalopodes
Calcaires Pseudolithographiques
Calcaires Lithés
Couches de Geissberg
Quaternary
Neogene
Paleogene
Upper Cretaceous
Lower Cretaceous
Upper Jurassic
Mid. Jurassic
Lower Jurassic
Triassic
1. Salève Mountain
2. Prapont
3. Morillon
4. Valefin
5. Roche Blanche
6. Reculet Nord
7. Col de la Faucille

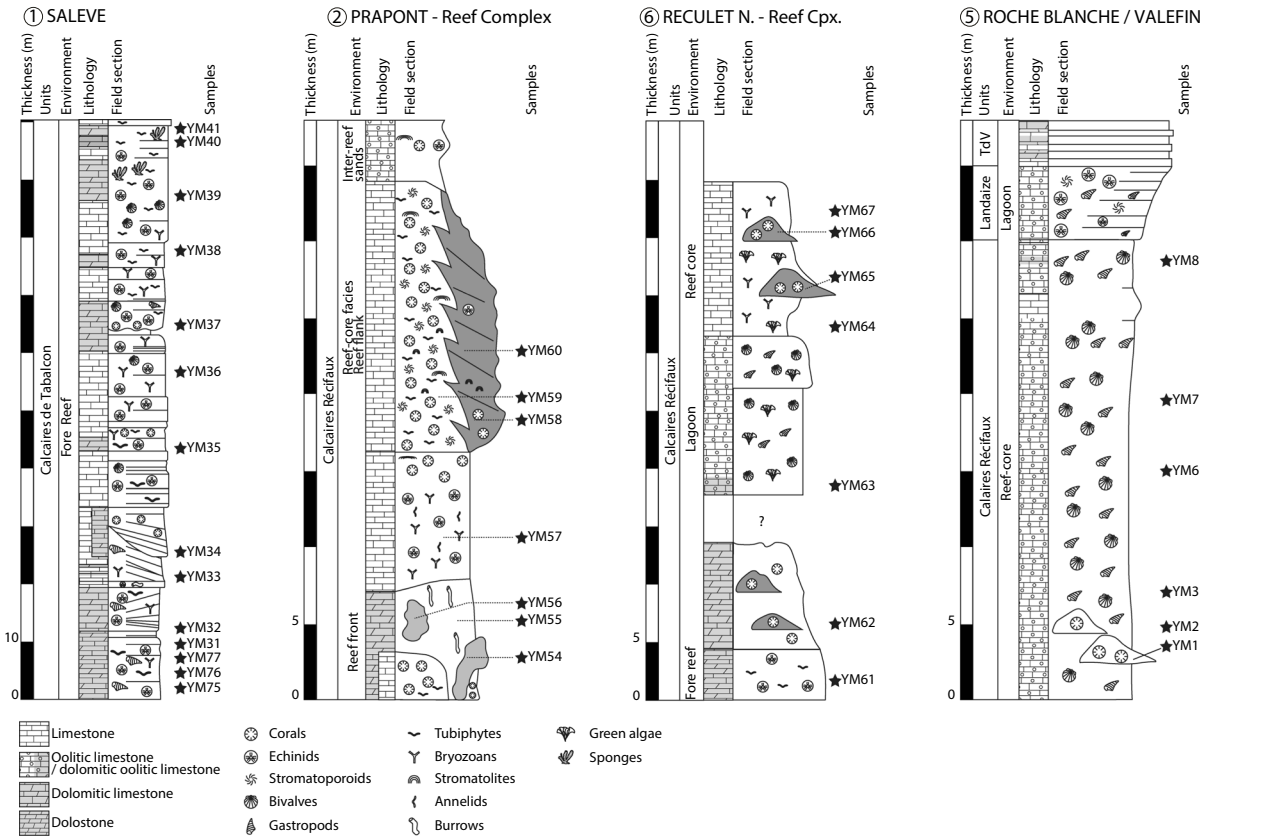
① SALEVE
② PRAPONT - Reef Complex
⑥ RECULET N. - Reef Cpx.
⑤ ROCHE BLANCHE / VALEFIN
Thickness (m)
Units
Environment
Lithology
Field section
Samples
Calcaires de Tabalcon
Fore Reef
Calcaires Récifaux
Reef-core facies
Reef flank
Inter-reef sands
Reef front
Reef core
Lagoon
Fore reef
TdV
Landaize
Reef-core
Limestone
Oolitic limestone / dolomitic oolitic limestone
Dolomitic limestone
Dolostone
Corals
Echinids
Stromatoporoids
Bivalves
Gastropods
Tubiphytes
Bryozoans
Stromatolites
Annelids
Burrows
Green algae
Sponges

◀**Fig. 1** Simplified geological map of the Geneva Basin and its vicinity. White stars represent location of the studied outcrops. (1) Salève Mountain; (2) Prapont; (3) Morillon; (4) Valefin; (5) Roche Blanche; (6) Le Reculet Nord and (7) Le Col de la Faucille. On the right, a synthetic log of the Upper Jurassic units as exposed in Mount Vuache. Stratigraphic logs modified from Makhloufi et al. (2018) for: the *Calcaires de Tabalcon* unit the Salève Mountains, modified from Deville (1990). The reef-front and reef-core sections of the *Calcaires Récifaux* in the Prapont section, modified from Fookes (1995). The top of the *Calcaires de Tabalcon* and the *Calcaires Récifaux* in the Reculet Nord section, modified after Meyer (2000). The *Calcaires Récifaux, Calcaires de Landaize* and *Tidalites de Vouglans* (TdV) unit in the Roche Blanche and Valefin sections modified after Makhloufi et al. (2018)

material including blocky calcite ($n = 12$), dolomite ($n = 24$), fracture infilling calcite ($n = 16$) and karst infilling calcite ($n = 5$). In total, 83 samples were collected for oxygen and carbon stable isotope geochemistry and 11 (blocky calcite $n = 6$, early dolomite $n = 3$, dolomite $n = 2$) for strontium isotope geochemistry. The reader is referred to Makhloufi et al. (2018) for a description of non-dolomitic cement not discussed here.

Cathodoluminescence analysis was completed using an ERI-MRTech-optical cathodoluminescence microscope with a cold cathode mounted on an Olympus BX41 petrological microscope at the Department of Earth Sciences (University of Geneva, Switzerland). The beam conditions were 15–18 kV at 120–200 mA with an unfocused beam of approximately 1 cm. The observation chamber has a residual pressure of ca. 50 mTorr. The samples were non-coated. A carbon coating (ca. 15 nm) by carbon thread evaporation was used prior to imaging with a Jeol JSM 7001F Scanning Electron Microscope (S.E.M., Department of Earth Sciences—University of Geneva, Switzerland). The semi-quantitative analyses and mapping were obtained with an EDS detector coupled with the JED 2300 software.

For C and O isotopes, carbonate powders were reacted with 100% phosphoric acid at 70 °C using a Gasbench II connected to a ThermoFisher Delta V Plus mass spectrometer at the Department of Geography and Earth Sciences (Friedrich-Alexander-University of Erlangen-Nürnberg, Germany). All values are reported relative to V-PDB. Reproducibility and accuracy were monitored by replicate analysis of laboratory standards calibrated by assigning $\delta^{13}C$ values of +1.95‰ to NBS19 and − 46.6‰ to LSVEC and $\delta^{18}O$ values of − 2.20‰ to NBS19 and − 23.2‰ to NBS18. Reproducibility for $\delta^{13}C$ and $\delta^{18}O$ was ± 0.06 and ± 0.06 (1 std. deviation), respectively. Oxygen isotope values of dolomite were corrected using the phosphoric acid fractionation factors given by Kim et al. (2007) and Rosenbaum and Sheppard (1986).

For Sr isotopes, a few mg of powdered carbonate material were dissolved in 2.2 M high purity acetic acid during 1 to 2 h at room temperature in conical shaped 2 ml vials. The solutions were centrifuged, and the supernatant was recovered and transferred to Teflon vials, where it was dried down on a hot plate. The residue was redissolved in a few drops of 14 M HNO3 and dried down again, before Sr separation from the matrix using a Sr-Spec resin. The Sr separate was redissolved in 5 ml of ∼ 2% HNO3 solutions and ratios were measured using a Thermo Neptune PLUS Multi-Collector ICP-MS in static mode. The $^{88}Sr/^{86}Sr$ (8.375209) ratio was used to monitor internal fractionation during the run. Interferences at masses 84 (^{84}Kr), 86 (^{86}Kr) and 87 (^{87}Rb) were also corrected in-run by monitoring ^{83}Kr and ^{85}Rb. The SRM987 standard was used to check external reproducibility, which on the long-term (more than 100 measurements for 1 year) was 10 ppm. The internally corrected $^{87}Sr/^{86}Sr$ values were further corrected for external fractionation (due to a systematic difference between measured and a nominal standard ratio of the SRM987 of $^{87}Sr/^{86}Sr = 0.710248$: McArthur et al. 2001) by a value of − 0.025‰ per amu.

4 Results

4.1 Sedimentology and petrography

A comprehensive description of the sections measured in this study and sample locations are presented in Makhloufi et al. (2018) where readers can refer to figure 1 and 2 as supplementary data. The *Calcaires de Tabalcon* unit is characterized by pluridecimetric beds, about 20 meters thickness, separated by discrete dry joints. This unit can easily be observed in the Etiollet section were the four sedimentologic facies described by Deville (1988) were sampled: (1) a micritic facies with accumulation of micropeloids and open marine, low energy, outer shelf associated fauna, locally dolomitized (2) a bioclastic facies subdivided in two and consisting of wackestone and packstone to grainstone, associated with peri-reefal fauna, then a (3) bioclastic facies consisting of peri-reefal and reefal associations with extraclasts, some being decametric in size, composed of corals, gastropods, lagoonal mudstones, high-energy grainstones and fore-reef biomicrites (Fig. 2a) and finally (4) a dolomitized bindstone facies composed of siliceous sponges and including pyrite-limonite incrustation (Fig. 2b). In the Reculet Nord section, the *Calcaires de Tabalcon* is characterized by a dolomitized limestone consisting of medium to coarse, euhedral, highly coalescent replacive rhombs that obliterated the initial fabric (Fig. 2c). Most of the rhombs display a dark cloudy core and clear outer rim. The *Calcaires Récifaux* unit was

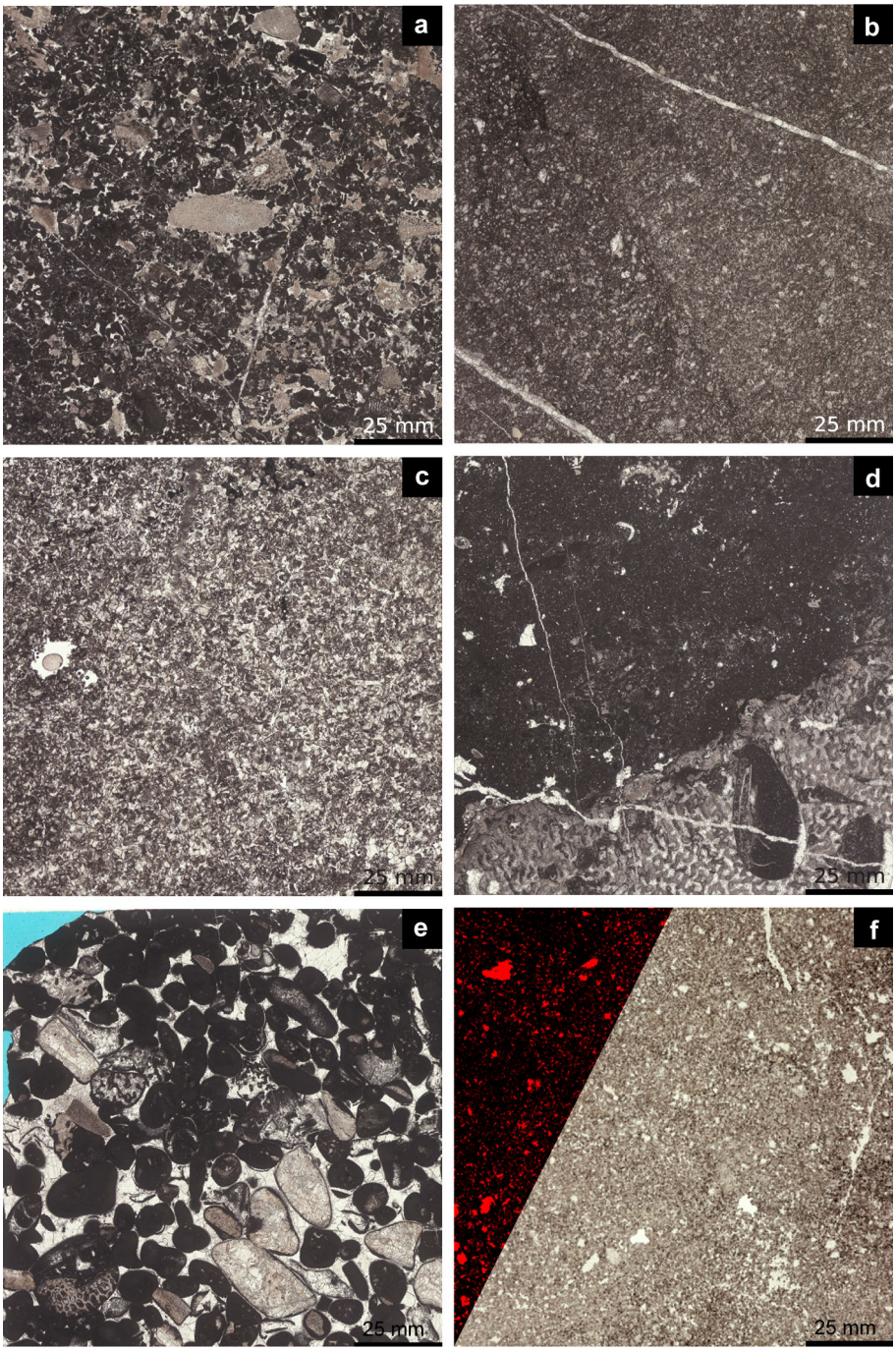

Fig. 2 Photomicrographs of the main facies observed in the Kimmeridgian–Tithonian limestones of the Geneva Basin. **a** packstone to grainstone facies in the Calcaire de Tabalcon unit; **b** dolomitized boundstone in the Calcaires de Tabalcon unit; **c** medium sized, fabric destructive, sucrosic dolomite in the Calcaires de Tabalcon unit; **d** wackestone with microsolenoid coralsin the Calcaires Récifaux unit; **e** oncoid grainstone with calcite spar cement in the Calcaires de Landaize unit and **f** fine to medium sized, fabric destructive, sucrosic dolomite in the Tidalites de Vouglans unit. On the left, the complex, vuggy, porosity is filtered in red and amounts to 12.5% of the total image

studied in the Prapont, Valefin, Roche Blanche and Reculet Nord section, the reef front deposits exhibit beige wackestone with microsolenoid corals, stromatoporoids, bryozoans and rare foraminifers, along with oncoids and micropeloids that can be associated with microbial crusts (Fig. 2d). Lateral variations at small scale are typical in these deposits as large dolomitized patches can be observed along. Moldic and intergranular porosity as well as centimetric to decimetric vugy pores are common. The *Calcaire de Landaize* unit was studied in the Col de la Faucille, Valefin, and Roche Blanche sections and exhibits limestone beds composed of a beige oncoid grainstone with sparitic calcite cementation and no evidence of dolomitization (Fig. 2e). The *Tidalites de Voulgans* unit was mainly studied in the Roche Blanche and Valefin sections. There, the unit present submetric limestone beds and marly to dolomitic interbeds. The dolomitic interbeds are characterized by fine to medium, euhedral, and subhedral crystals that obliterated the initial fabric (Fig. 2f). Based on petrographic, specifically using crystal geometries, sizes,

crosscutting relations and isotopic signatures, two types of dolomites have been identified along the Kimmeridgian-Tithonian succession studied.

4.2 Dolomites and dedolomites petrography

4.2.1 Type 1 dolomites

Type 1 dolomite is composed of fine to medium, euhedral to subhedral, replacive rhombs. Dolomitization produced either isolated rhombs floating in a micritic matrix or euhedral to subhedral textures. Under non-polarized light, crystals generally display a cloudy core and a clear rim. Under CL dolomites display a non-luminescent dark core. Two stages of dolomitization can be distinguished (Fig. 3). Type 1a (T1-a) exhibits fine euhedral clear rhombs. Under CL it displays non-luminescent core and zoned, bright red luminescent overgrowth as well as replacive features (Fig. 3a, b). Calcite replacement of dolomite is also observed under S.E.M. (Fig. 4a, b, c). Type 1b (T1-b) exhibits fine to medium euhedral to subhedral rhombs displaying a dull red luminescence with rare zonations and locally a non-luminescent center (Fig. 3 c). Locally T1-b is affected by microfractures (Fig. 4c). T1-a dolomites are therefore recognized by smaller crystal size and brighter luminescence under CL.

E.D.S. analyses highlighted chemical differences between the host limestone and the replacive dolomite (Fig. 4c). Type 1 de-dolomites (T1-D) consist of (1) rhomb-shaped pores with remaining dolomites rims or dolomites patches on the borders including remains of dolomite crystals in the mottles (Fig. 3d). Location, geometry and size of T1-D correspond to those of early dolomites T1. Under CL, the remnants of partially dissolved dolomite crystals still exhibits dull-luminescent zonations when present. T1-dedolomites are characterized

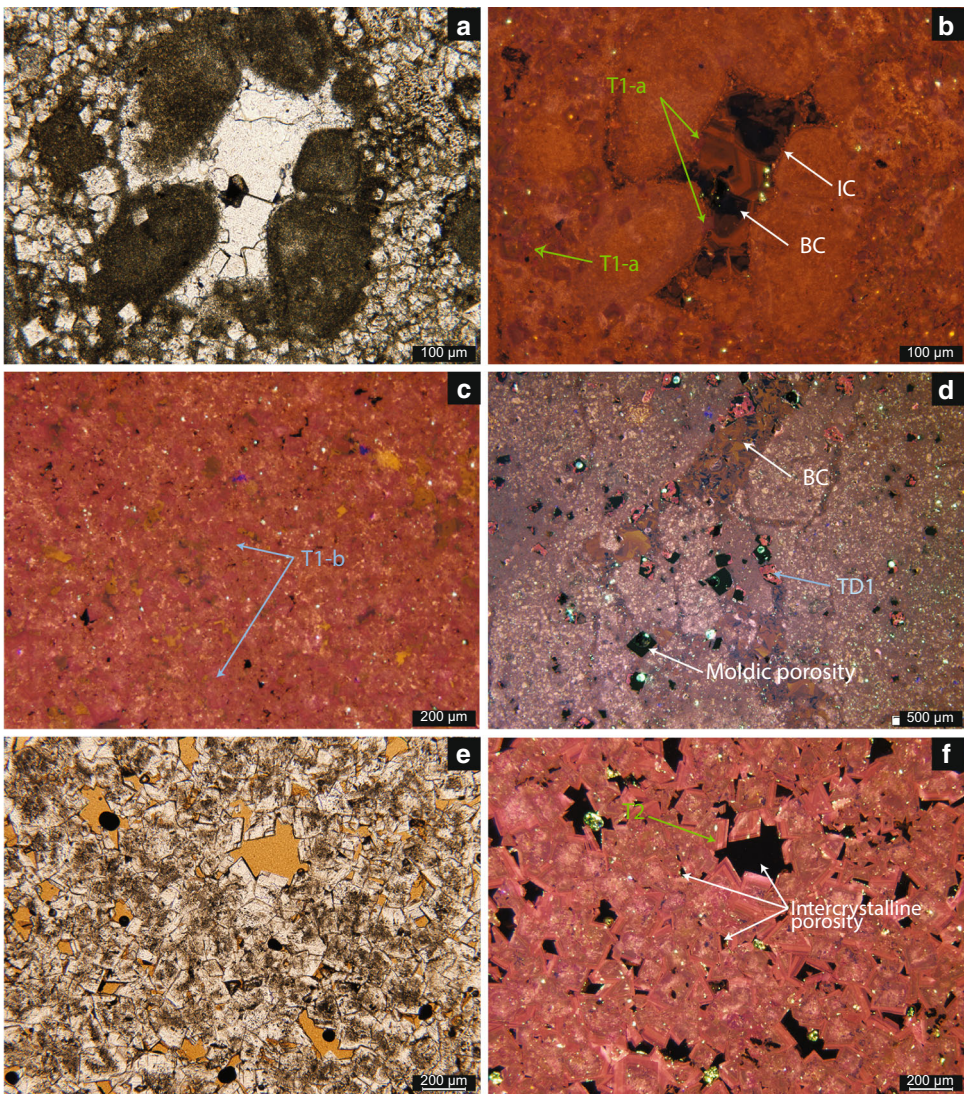

Fig. 3 Optical microscopy and CL on thin sections. **a** partial early dolomitization replacing both the micritic matrix, grains and calcite cements observed in polarized non-analyzed light under optical microscopy; **b** same thin section under CL putting in evidence two types of calcite cement (isopachous IC and blocky calcite BC) as well as the T1-a fine to medium early dolomite; **c** CL photograph of the T1-b dolomite exhibiting medium rhombs with a dull red luminescence and rare thin zonations. The dark spots represent secondary moldic porosity; **d** CL Evidence the remaining dolomite TD1 in secondary moldic pore resulting from dolomite dissolution during dedolomitization; **e** optical microscopy under natural light of the fabric destructive sucrosic dolomite. The rhombs core appears cloudy due to the presence of inclusions while the outer rims appears clear. The yellow to brown areas are intercrystalline pores filled by resin used for thin section manufacturing and **f** same thin section under CL, the sucrosic dolomite T2 exhibiting thin zonation in the clear rims, evidence for chemical modification during precipitation

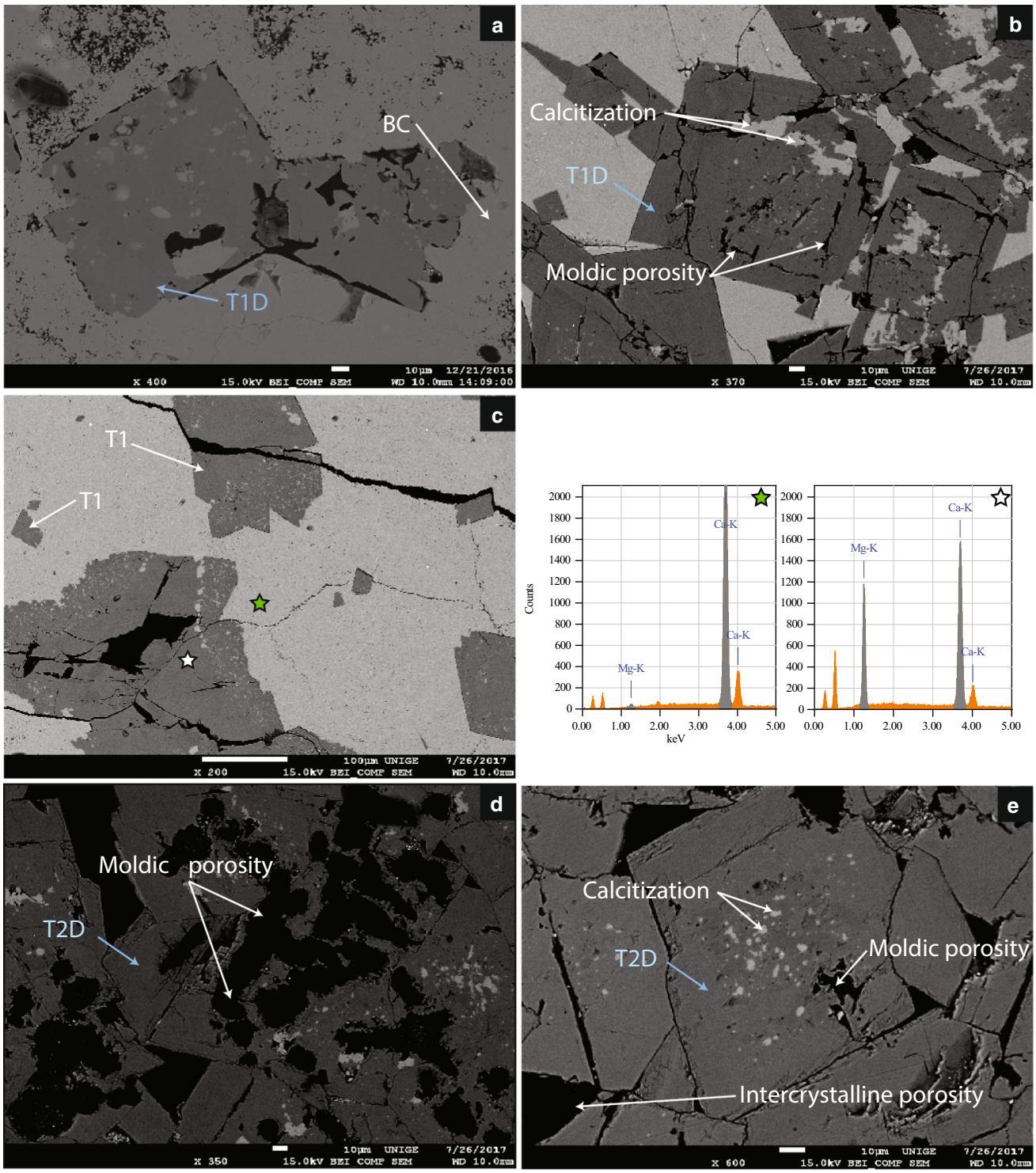

Fig. 4 S.E.M. images of samples affected by early dolomitization and dedolomitization. Calcite appears in light grey while dolomite appears in dark grey. **a** Blocky Calcite (BC) and T1 dedolomite (T1-D, dark grey). The dedolomite includes vuggy pores resulting from dissolution and replacement by calcite (light grey); **b** calcitization and intercrystalline microporosity in a T1 dedolomite; **c** replacive T1 dolomite and EDS analysis of the dolomite and micrite; **d** Sucrosic dedolomite (T2-D) showing important, large, intracrystalline vuggy pores but little amount of calcite replacement; **e** calcitization and intercrystalline microporosity in a T2 dedolomite, including intercrystalline porosity

by bright to dull luminescent, orange-colored, cores and bright to dull luminescent, red-colored, surrounding rims. Vuggy porosity is partially filled by calcite cement (Fig. 4a) and microporosity commonly follows the crystal zonations as observed under CL (Fig. 4b).

4.2.2 Type 2 dolomites

The second type of dolomite (T2) is composed of medium to coarse, euhedral to subhedral, fabric-destructive dolomite rhombs. Under non-polarized light, dolomite rhombs exhibit cloudy core and clear rim. Under CL, cloudy rombs are mostly non-luminescent while the clear rims exhibit red-colored, bright to dull luminescent zonations (Fig. 3e and f). The T2 dolomite exhibits significant intercrystalline porosity (10 to 12%, based on image analysis, Fig. 2f). This T2 dolomite has the same characteristics as "sucrosic" fabric-type dolomite. Type 2 de-dolomites (T2-D) exhibit intracrystalline microvugs (Fig. 4d) as well as selective dissolution and calcitization along their core/rim interface (Fig. 4e). Location, geometry and size of T2-D correspond to those of the T2 sucrosic dolomites. Under CL, the remaining dolomite filling the rhomb-shaped pores still exhibits dull-luminescent zonations when present. Calcitized dolomites are characterized by bright to dull luminescent, orange-colored, cores and bright to dull luminescent, red-colored, surrounding rims.

4.3 Dolomites and dedolomites geochemistry

4.3.1 Type 1 dolomites

The $\delta^{18}O$ values of T1-a dolomites range from − 0.3 to +1.5‰ (mean value: − 0.8‰) and the $\delta^{13}C$ values range from +2.3 to +3.2‰ (mean value: +2.8‰; Fig. 5 and Table 1). Due to the geometry and location of T1-b dolomites, it was not possible to sample separately this stage. Therefore, the analyzed powder is a mixture of a small fraction of T1-a dolomite and T1-b dolomites. However, as T1-b exhibits slightly larger crystals, we consider that the isotopic values are more representative of this stage. The $\delta^{18}O$ of values for T1-b dolomites range from − 4.6 to − 2.9‰ (mean value: − 3.6‰) and the $\delta^{13}C$ values range from +1.4 to +2.2‰ (mean value: +1.9‰, Fig. 5 and Table 1).

4.3.2 Type 2 dolomites

The $\delta^{18}O$ values of T2 dolomites range from − 4.3 to − 1.3‰ (mean value: − 2.9‰) and $\delta^{13}C$ values range from +2.1 to +2.7‰ (mean value: +2.3‰, Fig. 5 and Table 1). The $\delta^{18}O$ values of T1-D de-dolomites range from − 8.5 to − 6.9‰ (mean value: − 7.5‰) and $\delta^{13}C$ values range from − 4.9 to +2‰ (mean value: +0.4‰, Fig. 5 and Table 1). The ratio of $^{87}Sr/^{86}Sr$ range from 0.70710 to 0.70718 and from 0.70737 to 0.70752 for the T1 and T2 dolomites, respectively (Fig. 6). Only two T2 samples including de-dolomites were analyzed. Their $\delta^{18}O$ values are − 6.8‰ and − 6.5‰ and their $\delta^{13}C$ values − 1‰ and +0.9‰, respectively (Fig. 5).

5 Discussion

The following discussion focuses on the composition of dolomitizing fluids and the timing of dolomitization, using data from C, O and Sr isotopes. The discussion takes into account the interpretation of the paragenesis drawn from petrography in a previous study (Makhloufi et al. 2018). The discussion is extended to include comparison with dolomitization and dedolomitization scenarios reported from the Molasse Basin.

Some studies addressed critically the issue regarding the use of geochemical data based on cement sampling: the isotopic composition of dolomites discussed here represent samples consisting of pure dolomite or a mix of dolomite and the calcareous matrix. The latter case, the isotopic value represents a geochemical average of both phases present in the sample. This problem is common in such facies where samples exhibits small crystal sizes, making sampling pure dolomite difficult. However, previous studies acknowledged this bias and showed that bulk analysis can still provide insights on diagenetic processes, especially in Jurassic and Cretaceous carbonates (Joachimski1994; Plunkett 1997; Fouke et al. 2005; Rameil 2008).

5.1 Timing and origin of the early dolomitization

According to the interpretation of the paragenesis proposed in Makhloufi et al. (2018), the early dolomitization occurred in two phases: a first phase induced by a reflux type dolomitization and a second phase thought to result from shallow burial dolomitization.

The $^{87}Sr/^{86}Sr$ of the dolomite samples range from 0.70710 to 0.70752 (Fig. 6). All values for T1a dolomites fall within the range for Tithonian seawater (0.70700–0.70718, McArthur et al. 2001). This is compatible with the previously discussed origin of early dolomitization as the consequence of the diagenetic replacement of micrite during shallow seepage reflux and/or evaporitic resulting brines at near surface for the Kimmerdigian-Tithonian of the Geneva Basin limestones (Makhloufi et al. 2018).

Estimating the $\delta^{18}O$ of dolomite precipitating in equilibrium with a pore fluid in function of the temperature requires the calculation of $\delta^{18}O$ composition of

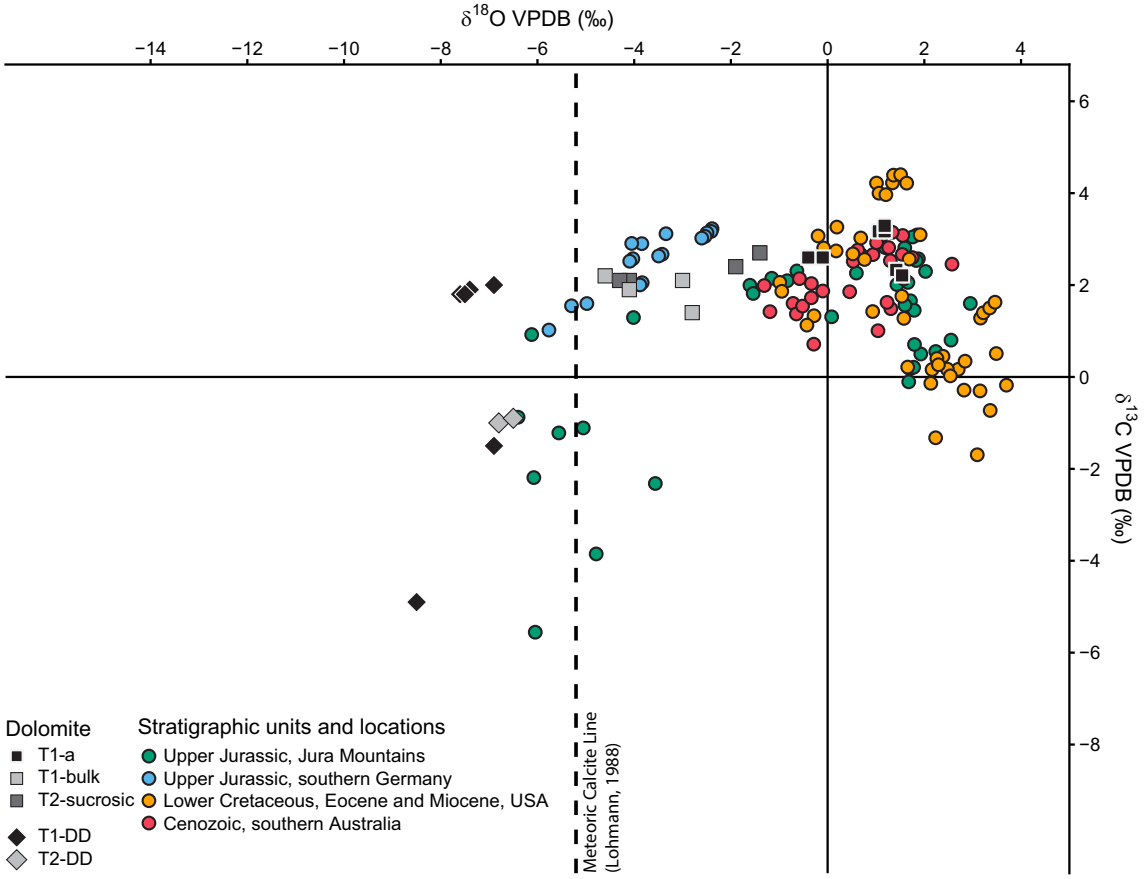

Fig. 5 Comparison of the isotopic composition measured in this study (grey to black symbols) and that of other studies compiled from the literature. Additional data of different types of dolomites. Green dots: Upper Jurassic of the Jura Mountains (Rameil 2008 and Baldermann et al. (2015). Blue dots: Upper Jurassic of southern Germany (Reinhold 1998). Orange dots: Mississippian, Lower Cretaceous, Eocene, and Miocene sucrosic dolomites in the U.S. (Choquette and Hiatt 2008). Red dots: Cenozoic sucrosic dolomites of southern Australia (Kyser et al. 2002). Raw values are available in the supplementary data

coprecipitated calcite and the numerical difference between the $\delta^{18}O$ composition of both dolomite and calcite ($\Delta\delta^{18}O_{dol\text{-}cal}$). A typical value of 3.8‰ for $\Delta\delta^{18}O_{dol\text{-}cal}$ is commonly used (Land 1992). Based on the equation from Friedman and O'Neil (1977), modified by Land (1985), $\delta^{18}O_{water}$ and $\delta^{18}O_{dolomite}$ (Suzuki et al. 2006; Yamamoto et al. 2018), the following formula is used:

$$\delta^{18}O_{water} = \delta^{18}O_{dolomite} - 2.78(10^6T^{-2}) - 0.91$$

where oxygen isotopic values are in VSMOW and temperature in kelvins. The conversion between the VPD-B and SMOW was performed using the equation of Coplen et al. (1983). With a $\delta^{18}O_{dolomite}$ composition from − 0.36 to +1.46‰ (Figs. 5 and 7a) for T1-a dolomites and Upper Jurassic seawater temperature at approximately 25 °C (~ 77 °F, Dromart et al. 2003; Blaise et al. 2014, 2015; Brigaud et al. 2008), the calculated $\delta^{18}O_{water}$ ranges from − 1.68 to +0.27‰ SMOW (Fig. 7a). Late Jurassic seawater oxygen composition are estimated to range from − 1.0 to − 1.2‰ (Shackleton 1975; Irwin et al. 1977; Hoefs 1987; Prestel 1990). Therefore, $\delta^{18}O_{water}$ calculated from the $\delta^{18}O$ composition of T1a dolomites are likely recording precipitation from original to slightly modified Late Jurassic seawater.

Carbon isotope values of T1a dolomite are close to the isotope composition of well-preserved Late Jurassic marine cements (Allan and Wiggins 1993) suggesting abiotic precipitation from seawater (Bone et al. 1992; Joachimski 1994). These values could be related to marine or nearly marine pore fluids (Nicolaides and Wallace 1997). Moreover, positive $\delta^{13}C$ values are incompatible with the influence of isotopically light carbon from organic matter, meteoric or mixed marine/meteoric water (Reinhold 1998). Therefore, the carbon isotopes values for T1a dolomite could be compared to published values of dolomites formed within shallow-burial marine environments (Mattes and Mountjoy 1980; Moore et al. 1988; Reinhold 1998; Machel and Anderson 1989). Moreover, the isotopic composition of the early dolomite is rather similar to that reported for the modern Abu Dhabi dolomites, which are

Table 1 $\delta^{18}O$ (V-PDB) and $\delta^{13}C$ (V-PDB) isotopic composition of dolomite and dedolomite cements

Name	Type	d13C	d18O
ym7	T1a dolomite	3.13	1.11
ym7	T1a dolomite	3.16	1.16
ym7	T1a dolomite	3.14	1.24
ym26	T1a dolomite	2.34	1.46
ym26	T1a dolomite	2.36	1.43
ym8	T1a dolomite	2.62	− 0.36
ym8	T1a dolomite	2.56	− 0.10
ym61	T2 dolomite	2.74	− 1.35
ym61	T2 dolomite	2.36	− 1.91
ym62	T2 dolomite	2.13	− 4.12
ym62	T2 dolomite	2.12	− 4.28
ym38	T1 bulk	2.08	− 3.04
ym38	T1 bulk	1.92	− 4.07
ym40	T1 bulk	1.42	− 2.80
ym35	T1 bulk	2.18	− 4.59
ym40	T1a DD	− 1.53	− 6.93
ym58	T1 DD	1.83	− 7.49
ym32	T1 DD	2.00	− 6.94
ym32	T1 DD	1.87	− 7.40
ym33	T1 DD	1.82	− 7.52
ym33	T1 DD	1.77	− 7.59
ym31	T1 DD	− 4.91	− 8.54
ym63	T2 DD	− 0.99	− 6.78
ym63	T2 DD	− 0.86	− 6.46

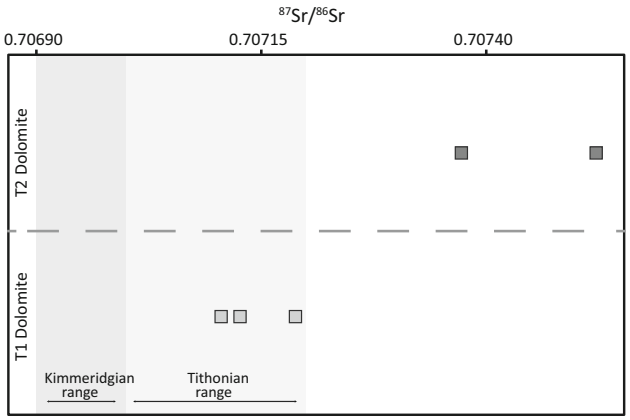

Fig. 6 Radiogenic strontium isotope composition of T1 dolomites and T2 dolomites. Kimmeridgian and Tithonian ranges for seawater strontium composition from McArthur et al. (2001)

the result of early diagenesis replacing magnesian calcite and aragonitic precursors, by direct precipitation under evaporitic conditions (Land and Hoops 1973; Staudt et al. 1994; Budd 1997; Warren 2000; Bontognali et al. 2014; Baldermann et al. 2015). Consequently, both the oxygen and the carbon isotopic values points to a marine or modified marine origin for the early dolomitization's parent fluid.

T1-b dolomites isotopic composition is significantly different from T1-a dolomites. The $\delta^{18}O$ values, ranging from − 4.59 to − 2.89‰, are more negative than the $\delta^{18}O$ values of T1-a dolomites previously discussed. Using the equation of Friedman and O'Neil (1977) with a temperature of 25 °C, the $\delta^{18}O_{water}$ calculated ranges from − 8.38 to − 4.16‰ (VSMOW, Fig. 7a), which are not compatible with $\delta^{18}O$ values of Late Jurassic seawater. Recrystallization of early, near surface to shallow dolomite could explain the lower $\delta^{18}O$ values by resetting the original isotopic composition of dolomite. Under CL T1-b displays red to dull luminescence, with thin zonations, typical for recrystallized dolomites (Cander et al. 1988; Nielsen et al. 1994; Machel 1997; Nader and Swennen 2004; Nader et al. 2007). The shift toward lower values of $\delta^{18}O$ could suggest recrystallization at elevated temperatures during successive burial (Nicolaides and Wallace 1997) or the influence of meteoric water (Banner et al. 1988; Gao 1990, Gao and Land 1991; Dorobek et al. 1993, Smith and Dorobek 1993; Warren 2000; Machel 2004; Nader et al. 2007). With $\delta^{13}C$ values ranging from +1.42 to +2.18‰, the composition of these dolomites deviates significantly from that of Late Jurassic seawater. Therefore, a potential influence of organic matter, meteoric or meteoric/marine mixed fluids cannot be ruled out. Given the petrographic evidence (Makhloufi et al. 2018), T1-b dolomites do not seem to have precipitated under temperature higher than 50 °C. Consequently, the influence of meteoric water through a mixture of buried seawater and meteoric water to explain the isotopic composition of T1-b appears more likely. Cretaceous meteoric water had a $\delta^{18}O_{water}$ composition of − 5‰ (SMOW; Prestel 1989). Therefore, the isotopic composition of a mixture between trapped seawater and meteoric likely ranged from − 5 to +1‰ (SMOW) for the dolomitizing fluid (Coplen 1982; Hoefs 1987; Reinhold 1998), which is more likely to be compared with the calculated $\delta^{18}O_{water}$.

The data presented in this study can be compared to those acquired in the Molasse Basin. Further to the northeastern part of Switzerland, the petrographic and isotopic characteristics of the early dolomites presented in Rameil (2008) are comparable to those of the present study (Fig. 7b). Rameil (2008) distinguished three types of early diagenetic dolomite: "T1-matrix dolomite", "T2-tidal flat dolomite" and "T3-burrow dolomite". The scenario proposed for the precipitation of the first two dolomites is a reflux-type dolomitization. The "T1–matrix dolomite" exhibits oxygen composition slightly more negative than that of T1-a dolomites in the present study, with an offset of about ∼ 1.5‰. Using the equation of Friedman and

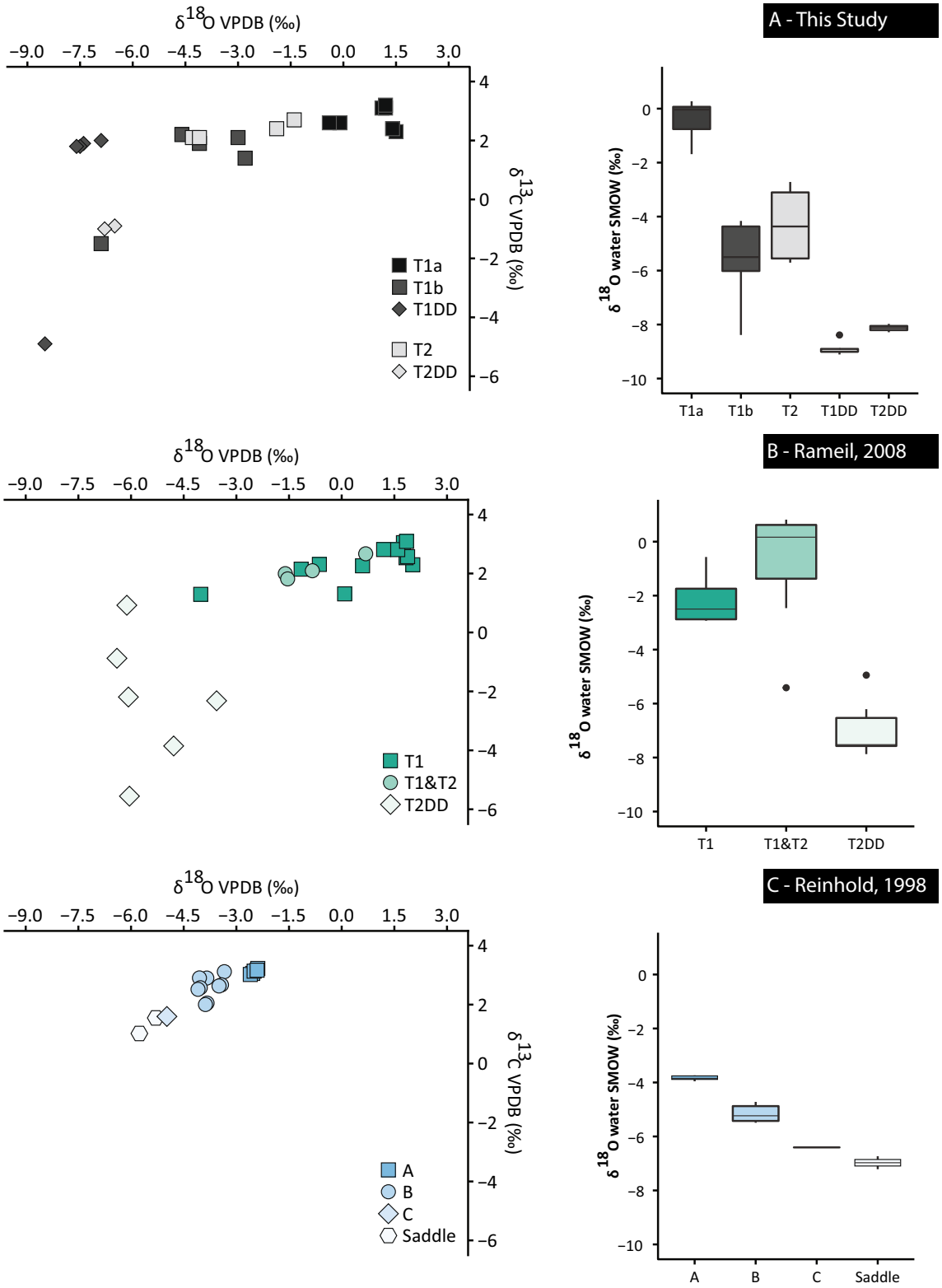
A - This Study
δ18O VPDB (‰)
δ13C VPDB (‰)
T1a
T1b
T1DD
T2
T2DD
δ18O water SMOW (‰)
B - Rameil, 2008
T1
T1&T2
T2DD
C - Reinhold, 1998
A
B
C
Saddle

◀**Fig. 7** Comparison between the isotopic compositions presented in this study with data from the Swabian Alb (southern Germany) dolomites and the Jura Mountains (northwest Switzerland and France) dolomites. The cross plots on the left represent the oxygen vs carbon isotopic composition. Boxplots on the right represent the results of the calculation of the initial isotopic composition of water derived from the equation of Friedman and O'Neil (1977) and modified by Land (1985). **a** data from this study; **b** isotopic compositions from Rameil (2008), where A refers to "matrix dolomite A", B and C to "recrystallized matrix dolomite B" and "recrystallized matrix dolomite C". **c** isotopic compositions from Reinhold (1998), where T1 refers to "Type 1 matrix dolomite", T1 and 2 refers to "mix of type-1 and type-2 tidal flat dolomites" and T2DD refers to "type-2 dedolomites"

O'Neil (1977) with a temperature of 25 °C, the $\delta^{18}O_{water}$ calculated values range from − 2.92 to − 0.56‰ (VSMOW, Fig. 7c). The average calculated $\delta^{18}O_{water}$ is − 2.12‰ (VSMOW) which is more negative than the estimated initial oxygen composition of around − 1.0‰ for Late Jurassic seawater (Shackleton 1975; Irwin et al. 1977; Hoefs 1987; Prestel 1990). Therefore, the "T1–matrix dolomite" was possibly precipitated from modified seawater. The same equation and parameters applied to the mixture of both the "T1–matrix dolomite" and "T2–tidal flat dolomite" result in calculated $\delta^{18}O_{water}$ values ranging from − 0.37 to − 5.41‰ (VSMOW, Fig. 7b). The average $\delta^{18}O_{water}$ composition is − 0.79‰ (VSMOW). This initial water composition is closer to the estimated Late Jurassic seawater oxygen composition and fits well with evaporitic brines evolving from initial seawater and inducing early dolomitization taking place directly at/or just beneath the sediment surface.

Eastward in the Molasse Basin, Reinhold (1998) identified six types of dolomites in the Upper Jurassic limestones of the Swabian Alb (southern Germany), among which three are early matrix dolomites. The oxygen isotopic composition of these different dolomites exhibits a progressive trend towards more negative $\delta^{18}O$ values ranging from − 2.39 to − 4.98‰ and $\delta^{13}C$ values ranging from 3.23 to 2.00‰ (Figs. 5 and 7c). Reinhold (1998) interprets the first stage of matrix dolomitization as deriving from slightly modified seawater and being related to pressure-dissolution during shallow burial at temperatures of at least 50 °C occurring during Upper Jurassic to Lower Cretaceous. While the geochemical data of Reinhold (1998) are comparable to those of the present study, the idiotopic euhedral texture and small grain size of early T1-a dolomites as well as the calculated $\delta^{18}O_{water}$ close to initial Late Jurassic seawater tend to indicate rather a low-temperature of formation (Sibley and Gregg 1987; Warren 2000; Meister et al. 2013). Furthermore, early dolomites observed in this study are not related to pressure-dissolution.

The comparison of the data presented in this study and the work of Rameil (2008) and Reinhold (1998) tends to indicate differential processes involved in the early dolomitization of the Upper Jurassic limestones in the Molasse Basin. In the western part of the basin (France and Switzerland), the early dolomitization originated from original to slightly modified Late Jurassic seawater. In the eastern part of the Molasse Basin, early dolomitization occurred slightly later than in the western part with a parent fluid that underwent further chemical modification through shallow burial.

5.2 Timing and origin of the late dolomitization

The two T2 sucrosic dolomite samples studied exhibit $^{87}Sr/^{86}Sr$ of 0.70737 and 0.70752. These values are out of range of Late Jurassic seawater composition. As discussed in Makhloufi et al. (2018), T2 sucrosic dolomite is most probably the result of shallow burial dolomitization originating from a mix between marine or evaporitic water and meteoric water. Therefore, the Sr signature of T2 sucrosic dolomite can possibly be modified by sub-surface fluids with radiogenic Sr such as meteoric groundwater and, therefore, would not be indicative of a timing of precipitation (Vahrenkamp and Swart 1990; Budd 1997; Wheeler et al. 1999; Suzuki et al. 2006; Yamamoto et al. 2018). The $\delta^{18}O$ values of T2 dolomites range from − 4.28 to -1.35‰ (mean value: − 2.92‰) and the $\delta^{13}C$ values range from +2.12 to +2.74‰ (mean value: +2.34‰, Fig. 5, 7a). Using the equation of Friedman and O'Neil (1977) with a temperature of 25 °C, the $\delta^{18}O_{water}$ values calculated range from − 5.70 to − 2.71‰ (VSMOW, Fig. 7a), which are not compatible with Late Jurassic seawater $\delta^{18}O$ values. However, unlike for early dolomitization, there is no petrographic evidence supporting a potential recrystallization. The presence of clear syntaxial overgrowth could reflect that the dolomitizing fluid which was potentially a mix between marine or evaporitic water and meteoric water. However, sucrosic dolomite precipitating from unmodified marine pore waters and presenting clear rims were reported by Kyser et al. (2002) in dolomite of the Cenozoic Gambier Limestone, Australia (red dots, Fig. 5). In this case, the isotopic composition of the sucrosic dolomite was interpreted as resulting from the precipitation of a fluid whose temperature and chemical composition did not vary through time. In the samples analyzed, the complex zonations in the outer rims are the consequence of intermittent changes in the chemical composition of the parent water. These zonations are interpreted as the result of a mix origin between marine and meteoric water (Banner et al. 1988; Cander et al. 1988; Cander 1994), excluding an unmodified marine pore water origin. Based on the petrography (Makhloufi et al. 2018) and geochemical data presented

herein, the formation of this T2 dolomite is interpreted as burial in origin, in agreement with the scenario proposed by Choquette and Hiatt (2008). In this model, the initial fabric is completely obliterated leaving important intercrystalline water-filled pore while the rigid framework formed by the dolomite cement tends to slow compaction. Further overgrowth of the dolomite cement filling the available pore space coarsen the initial dolomite texture as long as pore space is available.

5.3 Dedolomitization

Dedolomitization affected both the early and sucrosic dolomite but with different results. The early dolomite was greatly affected by dedolomitization with almost complete dissolution of dolomite resulting in the creation of moldic porosity (Fig. 3d) preserving the initial dolomitic rhomboedral shape. When the dissolution is not complete, remnant dolomite is observed at the edges of the moldic pores. The sucrosic dolomite was less affected, while locally presenting large dissolution gulfs (Fig. 4b); the main difference lies in the presence of calcite inside the remaining dolomite rhombs (Fig. 4a, c and d). Isotopic data shows strongly depleted oxygen composition with $\delta^{18}O$ values ranging from − 8.5 to − 6.9‰ for T1-D and from − 6.8 to − 6.5‰ for T2-D. Considering the carbon isotopic composition, values for T1-D are still within range of the Late Jurassic seawater composition, expect for one outlier, while values for T2-D are strongly depleted and negative in $\delta^{13}C$ (Fig. 57a). The calculated $\delta^{18}O_{water}$ of the dedolomites are also strongly negative with values ranging from − 9.1 to − 8.4‰ for T1-D and from − 8.3 to − 7.9‰ for T2-D. This negative $\delta^{18}O$water composition could be interpreted as the result of chemical resetting by $\delta^{18}O$-depletted meteoric waters (Rameil 2008). The vertical trend of the $\delta^{18}O$ and $\delta^{13}C$ isotopic composition (Fig. 5) is similar to the trend in the data of Rameil (2008) for northeastern Switzerland (Fig. 7c). This trend follows that the typical meteoric calcite line of Lohmann (1988) at $\delta^{18}O$ = − 5.3‰ (Nader et al. 2008; Rameil 2008), representing possible variations present within a single meteoric water system (Fig. 5, dashed line). Moreover, the oxygen isotopic composition is similar to values typically observed in meteoric vadose diagenesis (Videtich and Matthews 1980; Allan and Matthews 1982). Therefore, dedolomitization is most probably due to meteoric groundwater circulating and inducing dissolution of dolomite with or without precipitation of calcite in a two-step process.

In order to initiate dedolomitization, this groundwater has to be Ca^{2+} enriched and Mg^{2+} depleted. Shearman et al. (1961) and Rameil (2008) suggest that the meteoric dissolution of massive evaporites (gypsum and anhydrites), deposited during the Late Tithonian and Early Berriasian (Rameil 2005), may have led to the formation such fluids responsible for dedolomitization during their circulation. In this scenario, limestones from the vadose zone were flushed by meteoric water during short-termed exposure events that potentially led to the dissolution of dolomite during early diagenesis in relation to emersion events occurring shortly after deposition. The emersion events related to sea-level change would explain the large-scale distribution of dedolomitization as observed over long distances, from the Swiss-French Jura to the German basin. Another potential source of dedolomitizting fluid can be karst-related, Ca-enriched, meteoric water. The Early Barremian *Urgonien Blanc* unit is the last Mesozoic unit deposited in the Geneva Basin and serves as a substratum for the Paleogene deposits (Conrad 1969; Clavel and Charollais 1989; Blanc-Alétru 1995). This unit is composed mainly of micritic limestone and mostly known to exhibit important karstification filled with the *Grès sidérolithique* unit (Paleogene). The karstification of the Early and Late Cretaceous deposits in the Geneva Basin is attributed to the Paleocene emersion (Charollais et al. 2013). This important karstification could be a major source of Ca^{2+}-enriched water potentially initiating dedolomitization during its circulation in the underlying Upper Jurassic limestones. A similar scenario is proposed by Nader et al. (2008) for the dedolomitization of Jurassic dolostones from central Lebanon during the uplift and emergence of Mount Lebanon. The fact that the dedolomitized limestones exhibits open secondary moldic pores in outcrops, especially in sections such as the Prapont, where water circulation is still important, could indicate a late diagenetic dedolomitization most likely occurring during the uplift of the Jura Mountains in the Cenozoic. During this uplift, dissolution of evaporites, erosion of Cretaceous limestones, karstification of the Upper Barremian limestones and intensive flux of rainwater could contribute to a multistage process of dedolomitization. Complementary investigations in the Jura Mountain and, in a broader way in the Molasse Basin, are required in order to further constrain the timing and origin of the dedolomitization observed in the Upper Jurassic limestones of the Geneva Basin.

5.4 Heterogeneity of the dolomite fabrics

With regard to the paragenetic sequences described in Makhloufi et al. (2018), two different paths of dolomitization are identified in the Upper Jurassic limestones of the Geneva Basin. In both paths, the starting point is the early dolomitization originating from seepage-reflux (Figs. 8 and 9) during early diagenesis (eogenesis). From that point, a first path experienced the dissolution of $CaCO_3$ and coarsening of dolomite fabrics during late eogenesis to

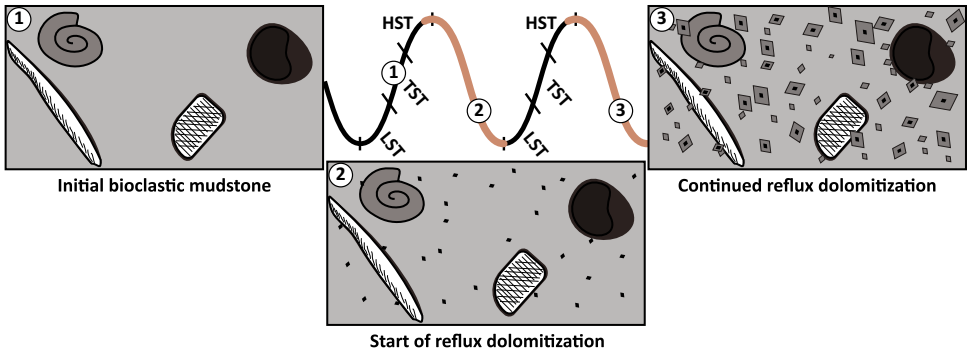

Fig. 8 Schemes of the early dolomitization. We consider an initial bioclastic mudstone (1) e.g. from lagoonal sediments. High frequency sea-level changes (2 and 3) will induce several pulses of downward migrating brines leading to (2) the nucleation of dolomite and (3) overgrowth of dolomite from the previously formed precursors

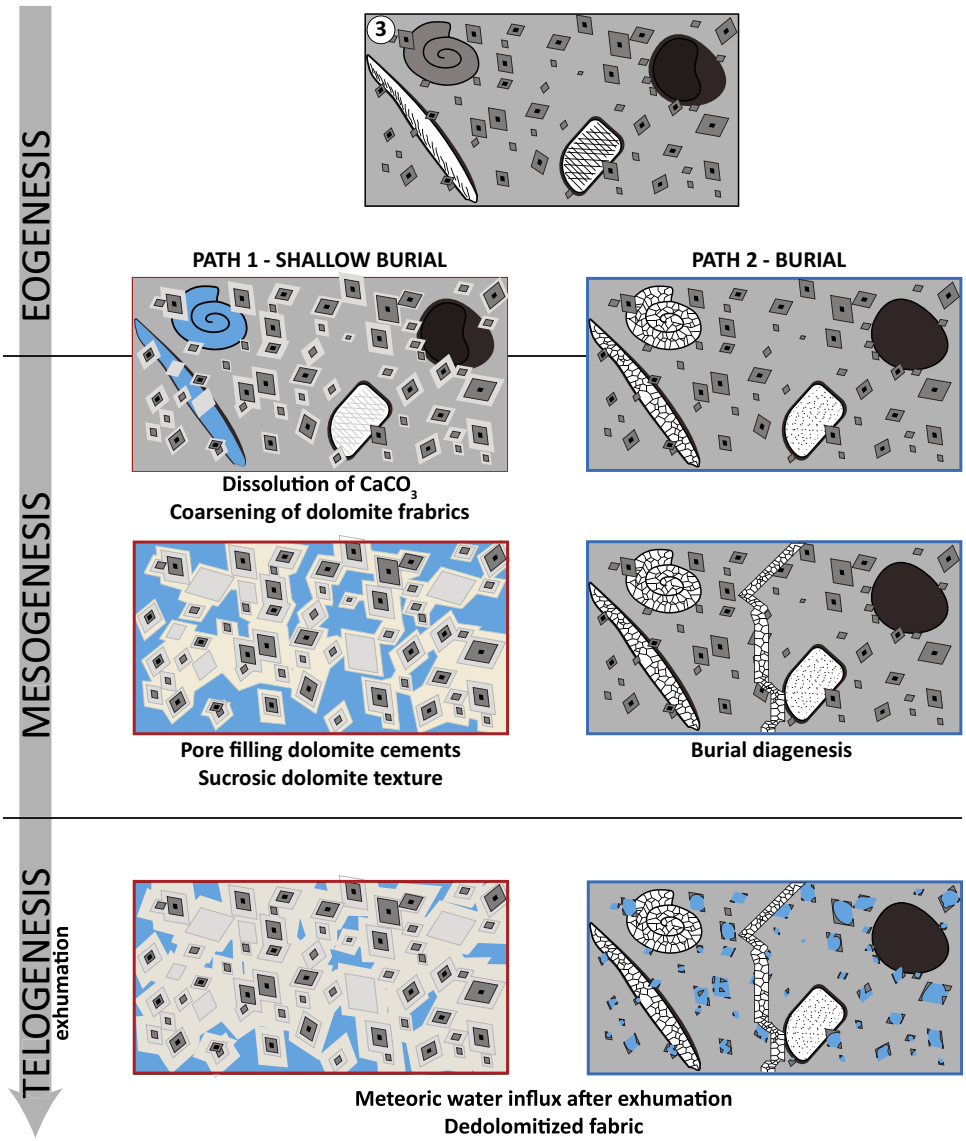

Fig. 9 Schemes of the dolomitization mechanics observed in the present study in relation to the overall diagenetic evolution. From the early diagenetic dolomitization initiated through seepage-reflux, two mechanisms were observed. In path 1, the limestone underwent dissolution of $CaCO_3$ and coarsening of the dolomite fabrics during late eogenesis and early mesogenesis (i.e. during shallow burial). The complete depletion of $CaCO_3$ as well as the overgrowth of dolomitic cements led to the formation of a fabric destructive sucrosic dolomite texture. During telogenesis (i.e. after exhumation) influx of meteoric seawater initiated dedolomitization. In path 2, early diagenetic dolomite precipitated until late eogenesis. During burial, the late dolomitic cement underwent recrystallization induced by a mixture of trapped initial seawater and circulating meteoric water. During telogenesis and exhumation, the same process of dedolomitzation as in path 1 produced the present-day observed dedolomitized fabric with secondary moldic pores

early mesogenesis. This path led to the formation of sucrosic dolomite with high intercrystalline porosity and pore filling dolomite cements overgrowing early dolomite precursors. The second path led to the formation of T1-b dolomites as the results of burial (potentially shallow) recrystallization by a mixture of trapped initial seawater and meteoric groundwater circulating during mesogenesis. Both paths ended after telogenesis and exhumation of the dolomitized limestones. At that point, dedolomitization led to the two dedolomitized fabrics observed. The sucrosic

dolomite was replaced after partial dissolution and, locally, precipitation of calcite. The early dolomitized texture where the initial micritic matrix was not completely replaced is characterized by secondary moldic porosity, still open in present-day outcropping rocks.

6 Conclusion

The Kimmeridgian and Tithonian sequences of the Geneva Basin recorded three different types of dolomities and two types of dedolomites. The three types of dolomites are distinguished by their geometry, grain-size, CL characteristics, stable isotope (O, C) and radiogenic (Sr) composition.

The first two types of dolomitization are interpreted as the results of early diagenesis. The first early dolomitization was produced by the replacement of micrite by dolomite during shallow seepage-reflux and/or evaporitic brines, migrating downward into the platform. This is in agreement with $^{87}Sr/^{86}Sr$ data supportive of a Tithonian age for dolomitization as well as oxygen and carbon isotopic values compatible with a non-modified seawater as the pore fluid for dolomitization. The second early dolomitization is the results of the same processes. However, isotope data points to the potential effect of (shallow) burial recrystallization involving a mixture of trapped initial seawater and meteoric water after their migration through limestones in the vadose zone. The third type of dolomite is characterized by a sucrosic fabric exhibiting important intercrystalline porosity. This type is most likely the result of burial dolomitization, resulting from precipitation of dolomitic syntaxial overgrowth over early dolomite precursors, a scenario supported by the oxygen and carbon isotopic composition and the $^{87}Sr/^{86}Sr$ out of range of Late Jurassic seawater composition.

Mechanisms and timing of dedolomitization are still not fully understood. From the data gathered in this study and by comparison with previous work at the regional and large scale, it is concluded that this process is the consequence of meteoric or modified meteoric water inducing dolomite dissolution. The implication of evaportites dissolution as a source of Ca^{2+} enriched fluid can neither discarded nor confirmed at the present stage of research. Late diagenesis after the uplift of the Jura and Salève Mountains is a more likely trigger for dedolomitizing fluid migration appears realistic.

The isotopic geochemical data of the present study and those gathered from the literature might provide a useful database for future research aiming to characterize multiphased dolomitized and dedolomitized limestones. The pathways of dolomitization and dedolomitization presented for the Geneva Basin and discussed with regards to the model proposed for the Upper Jurassic limestones at the regional and large scale is an important step towards an improved understanding of the diagenetic events that occurred in relation to large scale sea-level changes. Moreover, this study provides important insights into the assessment of the petrophysical properties distribution that will ultimately help in reservoir modeling, a crucial step for a further development of reusable energy in the Canton of Geneva and Switzerland.

Acknowledgements This study was funded by the Services Industriels de Genève (SIG) as a part of the GEothermy 2020 project. We are grateful to an anonymous reviewer for constructive comments on the earlier version of the manuscript. The Editor W. Winkler provided helpful advice which is thankfully acknowledged. We thank Michael M. Joachimski (University of Erlangen-Nürnberg, Germany) for carrying out the oxygen and carbon stable isotope analyses and Massimo Chiaradia (Department of Earth Sciences, University of Geneva) for providing the strontium isotope analyses. We also thank François Gischig, Nino Isabella Valenzi and Agathe Martignier from the Department of Earth Sciences, University of Geneva, Switzerland, for their help with thin section manufacturing, powder sampling, CL and S.E.M. imaging, respectively. Maud Brentini, Elme Rusillon, Jérôme Chablais (HydroGeo Environnement, Geneva) as well as Nicolas Clerc (GESDEC, Geneva) provided their help during fieldwork.

References

Allan, J. R., & Matthews, R. K. (1982). Isotope signatures associated with early meteoric diagenesis. *Sedimentology, 29*(6), 797–817.

Allan, J. R., & Wiggins, W. D. (1993). *Dolomite reservoirs: geochemical techniques for evaluating origin and distribution*. Tulsa: American Association of Petroleum Geologists.

Ayora, C., Taberner, C., Saaltink, M. W., & Carrera, J. (1998). The genesis of dedolomites: a discusion based on reactive transport modeling. *Journal of Hydrology, 209*(1–4), 346–365.

Baldermann, A., Deditius, A. P., Dietzel, M., Fichtner, V., Fischer, C., Hippler, D., et al. (2015). The role of bacterial sulfate reduction during dolomite precipitation: implications from Upper Jurassic platform carbonates. *Chemical Geology, 412,* 1–14.

Banner, J. L., Hanson, G. N., & Meyers, W. J. (1988). Water-rock interaction history of regionally extensive dolomites of the Burlington-Keokuk Formation (Mississippian): isotopic evidence. In V. Shukla & P. A. Baker (Eds.), *Sedimentology and Geochemistry of Dolostones* (Vols. 1-Book, Section, Vol. 43, pp. 97–113). SEPM Society for Sedimentary Geology. https://doi.org/10.2110/pec.88.43.0097.

Bernier, P. (1984). Les formations carbonatées du Kimméridgien et du Portlandien dans le Jura méridional: stratigraphie, micropaléontologie, sédimentologie. PhD dissertation, Lyon: Université de Lyon, Laboratoire de Géologie, 800 p.

Bernier, P., & Enay, R. (1972). Figures d'émersion temporaire et indices de sédimentation à très faible profondeur dans le Portlandien et le Kimméridgien supérieur (Calcaires en plaquettes) du Grand-Colombier-de-Culoz (Ain, France). *Bulletin de la Société Géologique de France, 7*(1–5), 281–292.

Blaise, T., Barbarand, J., Kars, M., Ploquin, F., Aubourg, C., Brigaud, B., et al. (2014). Reconstruction of low temperature (< 100 °C) burial in sedimentary basins: a comparison of geothermometer in the intracontinental Paris Basin. *Marine and Petroleum Geology, 53,* 71–87. https://doi.org/10.1016/j.marpetgeo.2013.08.019.

Blaise, T., Tarantola, A., Cathelineau, M., Boulvais, P., Techer, I., Rigaudier, T., et al. (2015). Evolution of porewater composition through time in limestone aquifers: salinity and D/H of fluid inclusion water in authigenic minerals (Jurassic of the eastern Paris Basin, France). *Chemical Geology, 417,* 210–227. https://doi.org/10.1016/j.chemgeo.2015.10.014.

Blanc-Alétru, M.-C. (1995). Importance des discontinuités dans l'enregistrement sédimentaire de l'urgonien jurassien: micropaléontologie, sédimentologie, minéralogie et stratigraphie séquentielle (PhD Thesis). Grenoble: Laboratoire de géologie de l'Université Joseph Fourier de Grenoble.

Bone, Y., James, N. P., & Kyser, T. K. (1992). Synsedimentary detrital dolomite in Quaternary cool-water carbonate sediments, Lacepede shelf, South Australia. *Geology, 20*(2), 109–112.

Bontognali, T. R. R., McKenzie, J. A., Warthmann, R. J., & Vasconcelos, C. (2014). Microbially influenced formation of Mg-calcite and Ca-dolomite in the presence of exopolymeric substances produced by sulphate-reducing bacteria. *Terra Nova, 26*(1), 72–77. https://doi.org/10.1111/ter.12072.

Braithwaite, C. J. R. (1991). Dolomites, a review of origins, geometry and textures. *Earth and Environmental Science Transactions of The Royal Society of Edinburgh, 82*(2), 99–112.

Brigaud, B., Pucéat, E., Pellenard, P., Vincent, B., & Joachimski, M. M. (2008). Climatic fluctuations and seasonality during the Late Jurassic (Oxfordian–Early Kimmeridgian) inferred from δ18O of Paris Basin oyster shells. *Earth and Planetary Science Letters, 273*(1), 58–67. https://doi.org/10.1016/j.epsl.2008.06.015.

Budd, D. A. (1997). Cenozoic dolomites of carbonate islands: their attributes and origin. *Earth-Science Reviews, 42*(1), 1–47. https://doi.org/10.1016/S0012-8252(96)00051-7.

Cander, H. S. (1994). An example of mixing-zone dolomite, middle Eocene Avon Park Formation, Floridan Aquifer system. *Journal of Sedimentary Research, 64*(3), 615–629.

Cander, H. S., Kaufman, J., Daniels, L. D., & Meyers, W. J. (1988). Regional dolomitization of shelf carbonates in the Burlington Keokuk formation (Mississippian), Illinois and Missouri: constraints from cathodoluminescent zonal stratigraphy. *Sedimentology and Geochemistry of Dolostones, 43,* 129–144.

Charollais, J.-J., Weidmann, M., Berger, J.-P., Engesser, B., Hotellier, J.-F., Gorin, G. E., et al. (2007). La Molasse du bassin franco-genevois et son substratum. *Archives des Sciences Genève, 60,* 59–174.

Charollais, J., Wernli, R., Mastrangelo, B., Metzger, J., Busnardo, R., Clavel, B., et al. (2013). Présentation d'une nouvelle carte géologique du Vuache et du Mont de Musieges (Haute-Savoie, France). Stratigraphie et tectonique. *Archives des Sciences Genève, 66,* 1–64.

Choquette, P. W., & Hiatt, E. E. (2008). Shallow-burial dolomite cement: a major component of many ancient sucrosic dolomites. *Sedimentology, 55*(2), 423–460.

Clavel, B., & Charollais, J. (1989). Stratigraphie de l'Hauterivien du Jura méridional. *Mémoires de la Société Neuchâteloise des Sciences Naturelles, XI,* 291–298.

Conrad, M. A. (1969). Les calcaires urgoniens dans la région entourant Genève. *Eclogae Geologicae Helvetiae, 61*(1), 1–79.

Coplen, T. (1982). Stable Isotope Hydrology: Deuterium and Oxygen-18 in the Water Cycle. *Eos, Transactions American Geophysical Union, 63*(45), 861–862.

Coplen, T. B., Kendall, C., & Hopple, J. (1983). Comparison of stable isotope reference samples. *Nature, 302*(5905), 236–238.

Deville, Q. (1988). Analyse sédimentologique et séquentielle des terrains les plus anciens du Salève: les traces d'un récif à la base (?) du Kimmeridgien. *Archives des sciences Genève, 40,* 65–84.

Deville, Q. (1990). Chronostratigraphie et lithostratigraphie synthétique du Jurassique supérieur et du Crétacé inférieur de la partie méridionale du Grand Saleve (Haute-Savoie, France). *Archives des Sciences. Genève*, *43*, 215–235.

Disler, C. (1914). Stratigraphie und Tektonik des Rotliegenden und der Trias beiderseits des Rheins zwischen Rheinfelden und Augst, Ph.D. dissertation, Basel: Universität Basel, 96 p.

Dorobek S.L., Smith T.M., Whitsitt P.M. (1993) Microfabrics and Geochemistry of Meteorically Altered Dolomite in Devonian and Mississippian Carbonates, Montana and Idaho. In R. Rezak & D.L. Lavoie (Eds.), *Carbonate Microfabrics*. Frontiers in Sedimentary Geology. New York, NY: Springer.

Dromart, G., Garcia, J.-P., Gaumet, F., Picard, S., Rousseau, M., Atrops, F., et al. (2003). Perturbation of the carbon cycle at the Middle/Late Jurassic transition: geological and geochemical evidence. *American Journal of Science, 303*(8), 667–707. https://doi.org/10.2475/ajs.303.8.667.

Enay, R. (1969). Le prétendu" Argovien" d'Entremont (Haute-Savoie). Découverte de la zone à Platynota (Kimméridgien inférieur) au Vuache (Jura méridional). *Société de Physique et d'Histoire Naturelle de Genève, 4*(1), 68–76.

Evamy, B. D. (1967). Dedolomitization and the development of rhombohedral pores in limestones. *Journal of Sedimentary Research, 37*(4), 1204–1215.

Favre, J. A., Risler, E., & Lossier, L. (1880). *Description géologique du canton de Genève*. A. Cherbuliez.

Fondeur, C., Gottis, M., Rouire, J., & Vatan, A. (1954). Quelques aspects de la dolomitisation au Jurassique en France. *XIXème Congr. Géol. Intern., Alger, 15,* 471–491.

Fookes, E. (1995). Development and eustatic control of an Upper Jurassic reef complex (Saint Germain-de-Joux, Eastern France). *Facies, 33*(1), 129–149.

Fouke, B. W., Schlager, W., Vandamme, M. G., Henderiks, J., & Van Hilten, B. (2005). Basin-to-platform chemostratigraphy and diagenesis of the Early Cretaceous Vercors Carbonate Platform, SE France. *Sedimentary Geology, 175*(1–4), 297–314.

Friedman, I., & O'Neil, J. R. (1977). Compilation of stable isotope fractionation factors of geochemical interest. *U.S. Geological Survey*, *440*(KK), 11.

Gao, G. (1990). Geochemical and isotopic constraints on the diagenetic history of a massive stratal, late Cambrian (Royer) dolomite, Lower Arbuckle Group, Slick Hills, SW Oklahoma, USA. *Geochimica et Cosmochimica Acta, 54*(7), 1979–1989.

Gao, G., & Land, L. S. (1991). Early Ordovician cool creek dolomite, middle arbuckle group, slick hills, SW Oklahoma, USA: origin and modification. *Journal of Sedimentary Research, 61*(2), 161–173.

Giorgioni, M., Iannace, A., D'Amore, M., Dati, F., Galluccio, L., Guerriero, V., et al. (2016). Impact of early dolomitization on multi-scale petrophysical heterogeneities and fracture intensity of low-porosity platform carbonates (Albian-Cenomanian, southern Apennines, Italy). *Marine and Petroleum Geology, 73,* 462–478.

Heim, A. (1922). Le sondage pour la recherche du pétrole à Challex (Ain). *Eclogae Geologicae Helvetiae, 17*(1), 115–123.

Hoefs, J. (1987). *Stable isotope geochemistry; Third, completely revised and enlarged*. New York: Springer.

Irwin, H., Curtis, C., & Coleman, M. (1977). Isotopic evidence for source of diagenetic carbonates formed during burial of organic-rich sediments. *Nature, 269*(5625), 209–213.

James, N. P., Bone, Y., & Kyser, T. K. (1993). Shallow burial dolomitization and dedolomitization of mid-Cenozoic, cool-water, calcitic, deep-self limestones, Southern Australia. *Journal of Sedimentary Research, 63*(3), 528–538.

Joachimski, M. M. (1994). Subaerial exposure and deposition of shallowing upward sequences: evidence from stable isotopes of Purbeckian peritidal carbonates (basal Cretaceous), Swiss and French Jura Mountains. *Sedimentology, 41*(4), 805–824.

Jones, B., Pleydell, S. M., Ng, K.-C., & Longstaffe, F. J. (1989). Formation of poikilotopic calcite-dolomite fabrics in the Oligocene-Miocene Bluff formation of Grand Cayman, British West Indies. *Bulletin of Canadian Petroleum Geology, 37*(3), 255–265.

Kenny, R. (1992). Origin of disconformity dedolomite in the Martin Formation (Late Devonian, northern Arizona). *Sedimentary Geology, 78*(1–2), 137–146.

Kim, S.-T., Mucci, A., & Taylor, B. E. (2007). Phosphoric acid fractionation factors for calcite and aragonite between 25 and 75 °C: Revisited. *Chemical Geology, 246*(3–4), 135–146.

Kyser, T. K., James, N. P., & Bone, Y. (2002). Shallow Burial Dolomitization and Dedolomitization of Cenozoic Cool-Water Limestones, Southern Australia: Geochemistry and Origin. *Journal of Sedimentary Research, 72*(1), 146–157. https://doi.org/10.1306/060801720146.

Land, L. S. (1985). The origin of massive dolomite. *Journal of Geological Education, 33*(2), 112–125.

Land, L. S. (1992). The dolomite problem: stable and radiogenic isotope clues. In N. Clauer & S. Chaudhuri S (Eds.), *Isotopic signatures and sedimentary records*. Lecture Notes in Earth Sciences (Vol. 43). Berlin: Springer.

Land, L. S., & Hoops, G. K. (1973). Sodium in carbonate sediments and rocks: a possible index to the salinity of diagenetic solutions. *Journal of Sedimentary Research, 43*(3), 614–617.

Lohmann K.C. (1988) Geochemical patterns of meteoric diagenetic systems and their application to studies of paleokarst. In N.P. James & P.W. Choquette (Eds.), *Paleokarst*. New York, NY: Springer.

Machel, H. G. (1997). Recrystallization versus neomorphism, and the concept of 'significant recrystallization'in dolomite research. *Sedimentary Geology, 113*(3–4), 161–168.

Machel, H. G. (2004). Concepts and models of dolomitization: a critical reappraisal. *Geological Society, London, Special Publications, 235*(1), 7–63.

Machel, H. G., & Anderson, J. H. (1989). Pervasive subsurface dolomitization of the Nisku Formation in central Alberta. *Journal of Sedimentary Research, 59*(6), 891–911.

Makhloufi, Y., Rusillon, E., Brentini, M., Moscariello, A., Meyer, M., & Samankassou, E. (2018). Dolomitization of the Upper Jurassic carbonate rocks in the Geneva Basin, Switzerland and France. *Swiss Journal of Geosciences, 111*(3), 475–500. https://doi.org/10.1007/s00015-018-0311-x.

Mattes, B. W., & Mountjoy, E. W. (1980). Burial dolomitization of the upper devonian miette buildup, Jasper National Park, Alberta. *SEPM Special Publication, 28,* 259–297.

McArthur, J. M., Howarth, R. J., & Bailey, T. R. (2001). Strontium isotope stratigraphy: LOWESS version 3: best fit to the marine Sr-isotope curve for 0–509 Ma and accompanying look-up table for deriving numerical age. *The Journal of Geology, 109*(2), 155–170.

Meister, P., Mckenzie, J. A., Bernasconi, S. M., & Brack, P. (2013). Dolomite formation in the shallow seas of the Alpine Triassic. *Sedimentology, 60*(1), 270–291. https://doi.org/10.1111/sed.12001.

Meyer, M. (2000). Le Complexe récifal Kimméridgien—Tithonien du Jura méridional interne (France), évolution multifactorielle, stratigraphique et tectonique. *Terre et Environment, 24,* 1–179.

Moore, C. H., Chowdhury, A., & Chan, L. (1988). Upper Jurassic smackover platform dolomitization northwestern Gulf of Mexico: a tale of two waters. *Sedimentology and Geochemistry of Dolostones, 43,* 753–778.

Nader, F. H., & Swennen, R. (2004). The hydrocarbon potential of Lebanon: new insights from regional correlations and studies of Jurassic dolomitization. *Journal of Petroleum Geology, 27*(3), 253–275.

Nader, Fadi H., Swennen, R., Ellam, R. M., & Immenhauser, A. (2007). Field geometry, petrography and geochemistry of a dolomitization front (Late Jurassic, central Lebanon). *Sedimentology, 54*(5), 1093–1120.

Nader, Fadi H., Swennen, R., & Keppens, E. (2008). Calcitization/dedolomitization of Jurassic dolostones (Lebanon): results from petrographic and sequential geochemical analyses. *Sedimentology, 55*(5), 1467–1485.

Nicolaides, S., & Wallace, M. W. (1997). Submarine cementation and subaerial exposure in Oligo-Miocene temperate carbonates, Torquay Basin, Australia. *Journal of Sedimentary Research, 67*(3), 397–410.

Nielsen, P., Swennen, R., & Keppens, E. (1994). Multiple-step recrystallization within massive ancient dolomite units: an example from the Dinantian of Belgium. *Sedimentology, 41*(3), 567–584.

Plunkett, J. M. (1997). *Early diagenesis of shallow platform carbonates in the Oxfordian of the Swiss Jura Mountains* (PhD Thesis). Fribourg: Université de Fribourg.

Prestel, R. (1989). Isotopengehalt von Kluft-Calciten aus dem Malm-Kern der Bohrung Saulgau GB 3. *Abh. Geol. Landesamt Baden-Württemberg, 13,* 161–180.

Prestel, R. (1990). *Untersuchungen zur Diagenese von Malm-Karbonatgesteinen und Entwicklung des Malm-Grundwassers in suddeutschen Molassebecken* (PhD Thesis). Stuttgart, Stuttgart.

Rameil, N. (2005). *Carbonate sedimentology, sequence stratigraphy, and cyclostratigraphy of the Tithonian in the Swiss and French Jura Mountains: a high-resolution record of changes in sea level and climate* (PhD Thesis). Fribourg: Université de Fribourg, 246 pp.

Rameil, N. (2008). Early diagenetic dolomitization and dedolomitization of Late Jurassic and earliest Cretaceous platform carbonates: a case study from the Jura Mountains (NW Switzerland, E France). *Sedimentary Geology, 212*(1–4), 70–85.

Reinhold, C. (1998). Multiple episodes of dolomitization and dolomite recrystallization during shallow burial in Upper Jurassic shelf carbonates: eastern Swabian Alb, southern Germany. *Sedimentary Geology, 121*(1–2), 71–95.

Rosenbaum, J., & Sheppard, S. M. F. (1986). An isotopic study of siderites, dolomites and ankerites at high temperatures. *Geochimica et Cosmochimica Acta, 50*(6), 1147–1150.

Schmoker, J. W., Krystinik, K. B., & Halley, R. B. (1985). Selected characteristics of limestone and dolomite reservoirs in the United States. *AAPG Bulletin, 69*(5), 733–741.

Shackleton, N. J. (1975). Paleotemperature history of the Cenozoic and the initiation of Antarctic glaciation: oxygen and carbon isotope analyses in DSDP Sites 277,279, and 281. *Initial Reports of Deep Sea Drilling Project, 29,* 743–756.

Shearman, D. J., Khouri, J., & Taha, S. (1961). On the replacement of dolomite by calcite in some Mesozoic limestones from the French Jura. *Proceedings of the Geologists' Association, 72*(1), 1–12.

Sibley, D. F., & Gregg, J. M. (1987). Classification of dolomite rock textures. *Journal of Sedimentary Petrology, 57*(6), 967–975.

Smith, T. M., & Dorobek, S. L. (1993). Alteration of early-formed dolomite during shallow to deep burial: Mississippian Mission Canyon Formation, central to southwestern Montana. *Geological Society of America Bulletin, 105*(11), 1389–1399.

Sommaruga, A. (1997). *Geology of the central Jura and the molasse basin: new insight into an evaporite-based foreland fold and thrust belt* (PhD Thesis). Université de Neuchâtel.

Staudt, W. J., Reeder, R. J., & Schoonen, M. A. A. (1994). Surface structural controls on compositional zoning of SO2−4 and SeO2−4 in synthetic calcite single crystals. *Geochimica et*

Cosmochimica Acta, 58(9), 2087–2098. https://doi.org/10.1016/0016-7037(94)90287-9.

Strasser, A. (1988). Shallowing-upward sequences in Purbeckian peritidal carbonates (lowermost Cretaceous, Swiss and French Jura Mountains). *Sedimentology, 35*(3), 369–383.

Strasser, A. (1994). Milankovitch cyclicity and high-resolution sequence stratigraphy in lagoonal–peritidal carbonates (Upper Tithonian–Lower Berriasian, French Jura Mountains). In P.L. de Boer, & D.G. Smith (Eds.), *Orbital forcing and cyclic sequences*. Special Publication International Association of Sedimentologists, pp. 285–301.

Suzuki, Y., Iryu, Y., Inagaki, S., Yamada, T., Aizawa, S., & Budd, D. A. (2006). Origin of atoll dolomites distinguished by geochemistry and crystal chemistry: Kita-daito-jima, northern Philippine Sea. *Sedimentary Geology, 183*(3), 181–202. https://doi.org/10.1016/j.sedgeo.2005.09.016.

Vahrenkamp, V. C., & Swart, P. K. (1990). New distribution coefficient for the incorporation of strontium into dolomite and its implications for the formation of ancient dolomites. *Geology, 18*(5), 387–391. https://doi.org/10.1130/0091-7613(1990)018%3c0387:NDCFTI%3e2.3.CO;2.

Videtich, P. E., & Matthews, R. K. (1980). Origin of discontinuity surfaces in limestones: isotopic and petrographic data, Pleistocene of Barbados, West Indies. *Journal of Sedimentary Research, 50*(3), 971–980.

Warrak, M. (1974). The petrography and origin of dedolomitized, veined or brecciated carbonate rocks, the 'cornieules', in the Fréjus region, French Alps. *Journal of the Geological Society, 130*(3), 229–245.

Warren, J. (2000). Dolomite: occurrence, evolution and economically important associations. *Earth-Science Reviews, 52*(1–3), 1–81.

Wheeler, C. W., Aharon, P., & Ferrell, R. E. (1999). Successions of late Cenozoic platform dolomites distinguished by texture, geochemistry, and crystal chemistry; Niue, South Pacific. *Journal of Sedimentary Research, 69*(1), 239–255. https://doi.org/10.2110/jsr.69.239.

Yamamoto, K., Ottinger, G., Al Zinati, O., Takayanagi, H., Yamamoto, K., & Iryu, Y. (2018). Geochemical, petrographical, and petrophysical evaluations of a heterogeneous, stratiform dolomite from a Barremian oil field, offshore Abu Dhabi (United Arab Emirates). *AAPG Bulletin, 102*(1), 129–152.